Imaging optical near fields at metallic nanoscale voids

P. D. Lacharmoise,[1,*] N. G. Tognalli,[2] A. R. Goñi,[1] M. I. Alonso,[1] A. Fainstein,[2] R. M. Cole,[3] J. J. Baumberg,[3] J. Garcia de Abajo,[4] and P. N. Bartlett[3]

[1]*Institut de Ciència de Materials de Barcelona-CSIC, Esfera UAB, 08193 Bellaterra, Spain*

[2]*Centro Atómico Bariloche-Instituto Balseiro, C.N.E.A., 8400 San Carlos de Bariloche, Río Negro, Argentina*

[3]*Cavendish Laboratory, University of Cambridge, Cambridge CB3 0HE, United Kingdom*

[4]*Instituto de Óptica, CSIC, Serrano 121, 28006 Madrid, Spain*

(Received 20 May 2008; revised manuscript received 14 July 2008; published 15 September 2008)

Direct imaging of the electromagnetic fields generated by plasmon excitation at gold nanoscale voids is achieved with high spatial resolution using scanning near-field optical microscopy (SNOM). The spatial intensity distribution of the electromagnetic field in spherical Au void structures strongly depends on the light excitation wavelength and on the diameter and degree of truncation of the voids. Comparing the SNOM results with reflectivity measurements and boundary element calculations allows for a clear identification of the plasmon modes being activated in each case. The unique mapping of the high-field regions provides key information for the use of void nanostructures as substrates for surface-enhanced Raman scattering.

DOI: 10.1103/PhysRevB.78.125410 PACS number(s): 68.37.Uv, 73.20.Mf, 72.15.Rn, 81.07.−b

I. INTRODUCTION

The field of plasmonics has experienced recently a rapid growth[1] due to the crucial role that plasmons play in a variety of disciplines such as near-field photonics,[2] optical switching,[3] and surface-enhanced Raman spectroscopy (SERS).[4] While more work concentrates on metallic nanoparticles, an alternative nanovoid (antiparticle) geometry has been successfully highlighted.[5] These ordered nanocavities allow for tuning plasmon modes from the visible to the near infrared with unsurpassed spatial homogeneity, repeatability, and time stability. The development of plasmonic devices has to rely on an increasing ability to fabricate and characterize metallic structures at the nanoscale, which, in turn, allows for a better understanding of the plasmon physics. In this respect, near-field optical microscopy (SNOM) appears as a particularly suitable technique for it is capable to probe electromagnetic fields generated at the metallic nanostructured surface by plasmon excitation.

Here we provide the first direct experimental, nanometer-resolution study of the spatial distribution of cavity plasmon modes by using resonant SNOM. The tailored cavity plasmon polaritons display atomiclike cavity centered or ring-shaped patterns, depending strongly on the light excitation wavelength and the size and degree of truncation of the gold voids. These modes are spectrally studied by reflectivity measurements and results are compared to boundary element calculations.[6] Rather of being restricted to void arrays, SNOM provides a unique mean for the direct optical characterization at the nanoscale of the strongly localized electromagnetic fields attained at any open plasmonic nanostructure.[7,8]

II. EXPERIMENT

The truncated nanovoid arrays are produced via a template self-assembly followed by an electrochemical Au deposition.[9,10] In this process, a solution of polymer spheres fills a thin fluid cell, which is made of a gold-coated glass slide, a clean glass slide, and sidewalls made from a 300 μm thick spacer of Parafilm. The gold slide is coated with cysteamine to reduce the contact angle of the aqueous liquid placed on the surface. This forms a sweeping meniscus tail as the fluid dries, which pulls spheres to the evaporation line where they form a close-packed monolayer domain. After template formation the sample is placed in an electrochemical plating bath. The degree of truncation can be finely controlled by the deposition time. Therefore, very clean, reproducible, and well-defined nanostructured surfaces are obtained over areas on the order of 1 cm^2. Moreover, by systematically retracting the sample from the solution during the metal deposition, it is possible to achieve different degrees of truncation in one single graded sample. A scanning electron micrograph of one nanovoid array is shown in Fig. 1(a) together with a three-dimensional (3D) image taken with the SNOM in topography mode. In order to properly

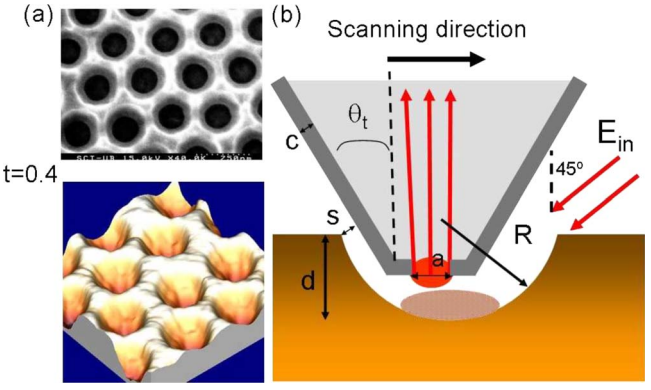

FIG. 1. (Color online) (a) SEM image of a $R=300$ nm void array together with a 3D image taken with the SNOM in topography mode. (b) Scheme of the experimental setup showing a sketch of the SNOM tip and parameters of the void cavity. R and d are the cavity radius and thickness, respectively. E_{in} represents the incident light. a and θ are the tip aperture and apex angle, respectively. a is nominally below 80 nm and $\theta \sim 40°$. c is the Al coating of the tip and s represents the tip-surface distance in feedback.

describe the different sample geometries, we define the normalized film thickness as $t=d/2R$, where d is the deposited Au film thickness and R is the void radius. When t is close to 0 the sample displays a quasi-two-dimensional (2D) patterned geometry. On the contrary, when t is close to 1, the surface has a 3D geometry with almost fully encapsulated voids.

A sketch of the experimental setup used for the SNOM imaging is shown in Fig. 1. A laser beam at 45° incidence is focused onto a spot of 5–10 μm in size at the sample surface. As we study arrays with void radii of $R=300$ nm and $R=400$ nm, the excited area contains tens of spherical cavities. An aluminum coated tip with an aperture diameter below 80 nm scans the excited area and collects the near field coming from the surface. The granular aluminum coating ensures that the tip surface is nonplasmonic. Since the scan is performed in noncontact mode using a tuning-fork technique, the tip-surface distance remains constant at 10–20 nm and both optical and topographical images from the sample can be obtained simultaneously.[11] Scans were performed at sufficiently slow pace (500 nm/s) looking for identical topographic images in forward and reverse scan directions to avoid any spurious distortion of the optical signal. Finally, the collected light from the near field goes to the acquisition system through an optical fiber connected to the tip. Since we use a far-field excitation, the optical field can couple with surface plasmons to form surface-plasmon polaritons (SPPs), leading to a stationary field distribution on the sample surface.[1,6,12,13] The SNOM tip probes this field distribution with a spatial resolution of about 50 nm roughly determined by the aperture diameter. However, tip size effects are to be considered, particularly for less truncated cavities with $t>0.6$, where the tip cannot enter completely into the void being insensitive to cavity modes. Moreover, if t is high enough, the tip may plug the cavity entrance shutting off illumination, i.e., plasmon excitation. We distinguish between propagating SPP modes on the surface of the structure and localized Mie-type modes inside the voids. Scanning near-field optical microscopy is a unique technique since it enables direct imaging of the optical field of these plasmon polaritons and their spatial distribution within the patterned structure with subwavelength spatial resolution.[11,14–16] We used SNOM to measure the dependence of the field distribution on excitation energy using different laser lines and the evolution of the plasmon-induced near-field distribution when t is progressively increased from 0.3 to 0.7 on a graded sample.

III. RESULTS AND DISCUSSION

Figure 2 shows SNOM images as a function of the excitation energy for a $R=300$ nm void structure at a normalized cavity thickness of $t=0.4$. The scans were performed by illuminating the same area of the sample with three different laser energies $E=2.41$ eV (green), 1.96 eV (red), and 1.58 eV (near infrared). In spite of the lower resolution, the topography sensed by the SNOM tip reproduces very well the scanning electron microscopy (SEM) images obtained on the same sample. Whereas topographic images exhibit complete

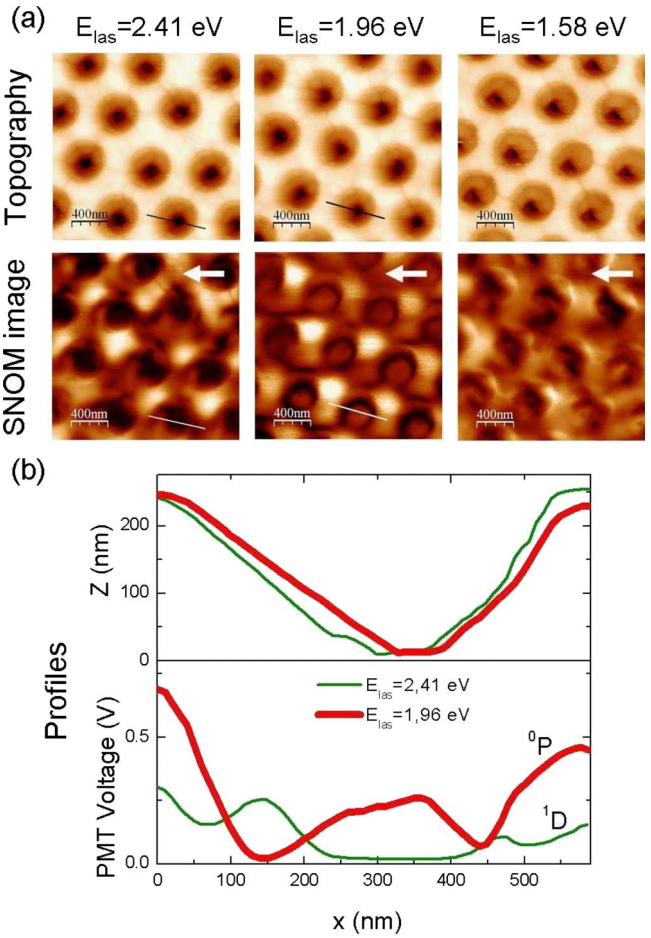

FIG. 2. (Color online) (a) Topography and SNOM images of a $R=300$ nm void array at $t=0.4$ obtained with different laser excitation energies. White arrows in the SNOM images indicate the direction of illumination. (b) Topography and SNOM line profiles along the black and white bars drawn on the images, respectively. Labels correspond to the assigned plasmon modes.

similarity, in SNOM they display unambiguous differences for the various laser lines. The specific direction of illumination, marked with arrows in Fig. 2(a), is responsible for the asymmetries of bright features and shadowed areas outside or at the top of the cavities. We now focus our attention on the signal collected at the voids. For $E=2.41$ eV a ring-shaped near-field signal is detected inside each cavity close to the void edges. When exciting at 1.96 eV, a completely different pattern develops with a void-centered bright signal apparent at the bottom of the cavities. Finally, no clear features can be identified at the voids for the 1.58 eV light.

Figure 2(b) shows a set of typical line profiles of both SNOM and topography signals along the lines marked on the images of Fig. 2(a) for 2.14 and 1.96 eV excitation. The lines along which the intensity cross cuts were performed have been chosen intentionally in order to stress the plasmon distribution inside the cavities, reducing at the same time the mixing with SPP contributions. As indicated in Fig. 1, the tip enters into a void keeping constant the distance s to the void rim. Thus, the tip moves along a funnel-like surface rather than a circular one, leading to topographic line profiles with

triangular shape such as the ones displayed in Fig. 2(b). The slope of the profiles corresponds to an angle of approximately 40°, which is very close to θ, the tip apex angle. Turning now to the SNOM profiles, the maximum intensity of the plasmon mode excited with 1.96 eV light occurs at the void center, whereas for 2.14 eV excitation there is a node at this position and the intensity distribution peaks at a void-centered ring of about 320 nm in diameter.

The spatial field distribution of the localized void plasmons is closely related to that of Mie-type modes. Mie theory gives the analytical solution to the Maxwell equations governing the scattering of a plane wave from a spherical particle in the limit of $R<\lambda$. The latter would correspond to a single void in a $t>1$ sample. In a real truncated cavity, these modes are influenced by the new geometry and can couple with incident light and interact with SPPs as well. The atomlike symmetry of the voids induces plasmon modes that resemble atomic orbitals with spherical harmonics components $Y^{l,m}$ with vectorial character. Thus, the mode labeling ${}^{m}L=^{0,1,\cdots}P,D,F,\ldots$ will be adopted hereafter. For plasmon-mode assignment we measured the reflectivity with s-polarized light at 45° incidence on a graded sample of $R=300$ nm nanovoids as a function of wavelength and thickness t [Fig. 3(a)]. In the figure, we mark with a horizontal line the thickness corresponding to the SNOM images taken at $t=0.4$ and with vertical lines the used laser wavelengths. It follows that at 2.41 and 1.96 eV the laser is almost in resonance with the plasmon modes labeled ${}^{1}D^{+}$ and ${}^{0}P$, respectively. For excitation at 1.58 eV, however, the resonance condition for the ${}^{1}P^{+}$ mode is only partially fulfilled. It is then reasonable to conclude that the SNOM signal maps out the intensity distribution of these plasmon modes which are being selectively excited with each laser line.

Let us now compare our measured cavity field distributions with theoretical data of the plasmon-field patterns.[6] The simulations were performed using a boundary element method in which the field inside a single isolated cavity is expressed in terms of the charges and currents of the structured surface. Figure 3(c) displays the calculated cross sections of the field distribution for the ${}^{0}P$ and ${}^{1}D$ modes. For 2.14 eV excitation the SNOM profile shown in Fig. 2(b) has maxima at either side of the center of the cavity. This mode picks up also a contribution from the coupling to the rim mode located at the cavity edge. Both discussed features clearly agree with the calculated ${}^{1}D^{+}$ intensity [see Fig. 3(c)]. In addition, the SNOM profile for 1.96 eV excitation exhibits a spherical intensity distribution spatially at the center of the truncated cavity. Once again, we find the very same characteristic for the calculated ${}^{0}P$ mode. We point out that this mode is activated in our experiments due to the 45° illumination. For the plasmon-field distribution measured with near IR light at 1.58 eV, the light is not strongly resonant with the cavity modes, leaving less contrasted void features mixed with residual interference patterns from the SPP plasmons on the top surface.

To study the dependence of the cavity modes on the degree of truncation of the void, we used a thickness graded sample with $R=400$ nm voids. SNOM and their corresponding topographic images are displayed in Fig. 4 for t ranging from ~0.3 to ~0.5. Unless otherwise indicated, we use the

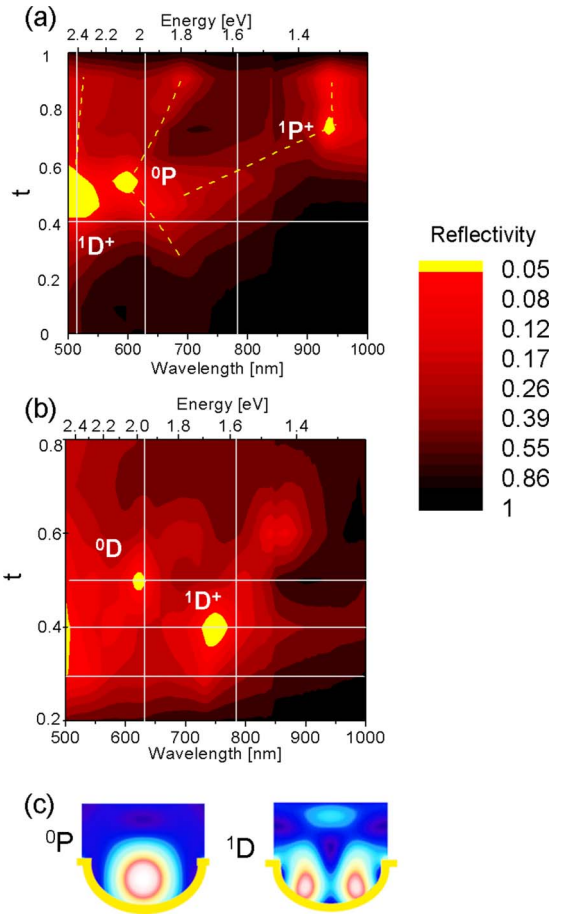

FIG. 3. (Color online) Measured s-polarized reflectivity at 45° incidence for (a) $R=300$ nm and (b) $R=400$ nm cavity structures graded from thin (bottom) to thick (top). The reflectivities of the graded samples with 800 and 600 nm of diameter were measured in 8 and 11 position steps, respectively. Dashed lines are guides to the eye to follow the ascribed Plasmon-mode evolution. Horizontal and vertical solid lines correspond to the normalized thickness and the excitation energies used in SNOM, respectively. (c) Cross section of the spatial plasmon distributions calculated for the ${}^{0}P$ and ${}^{1}D$ cavity modes in a $t=0.4$ void.

1.96 eV line for excitation. In Fig. 4, for each truncation degree we also show the topography and SNOM line profiles across a selected void in the rightmost panels. To help in the analysis we again show in Fig. 3(b) the reflectivity measured on this sample. At $t=0.3$ the SNOM image exhibits bright spots at the illuminated side of the void edges corresponding to the near-field enhancements due to SPP excitation and ring-shaped features centered at every void. This is consistent with the reflectivity data in Fig. 3(b), indicating that for 1.96 eV excitation we should be probing by SNOM the ${}^{1}D^{+}$ mode, although slightly out of resonance. The coupling to this mode, though, should be strongly enhanced for $t=0.4$ in accordance with the bright spot observed at 1.7 eV for this void thickness in reflectivity. Correspondingly, for $t=0.4$ the SNOM signal of the ring-shaped features is twice as strong as compared to $t=0.3$ (see the line profiles).

For $t=0.5$ the SNOM image displays instead a peak at the cavity center. We ascribe this intensity pattern to the obser-

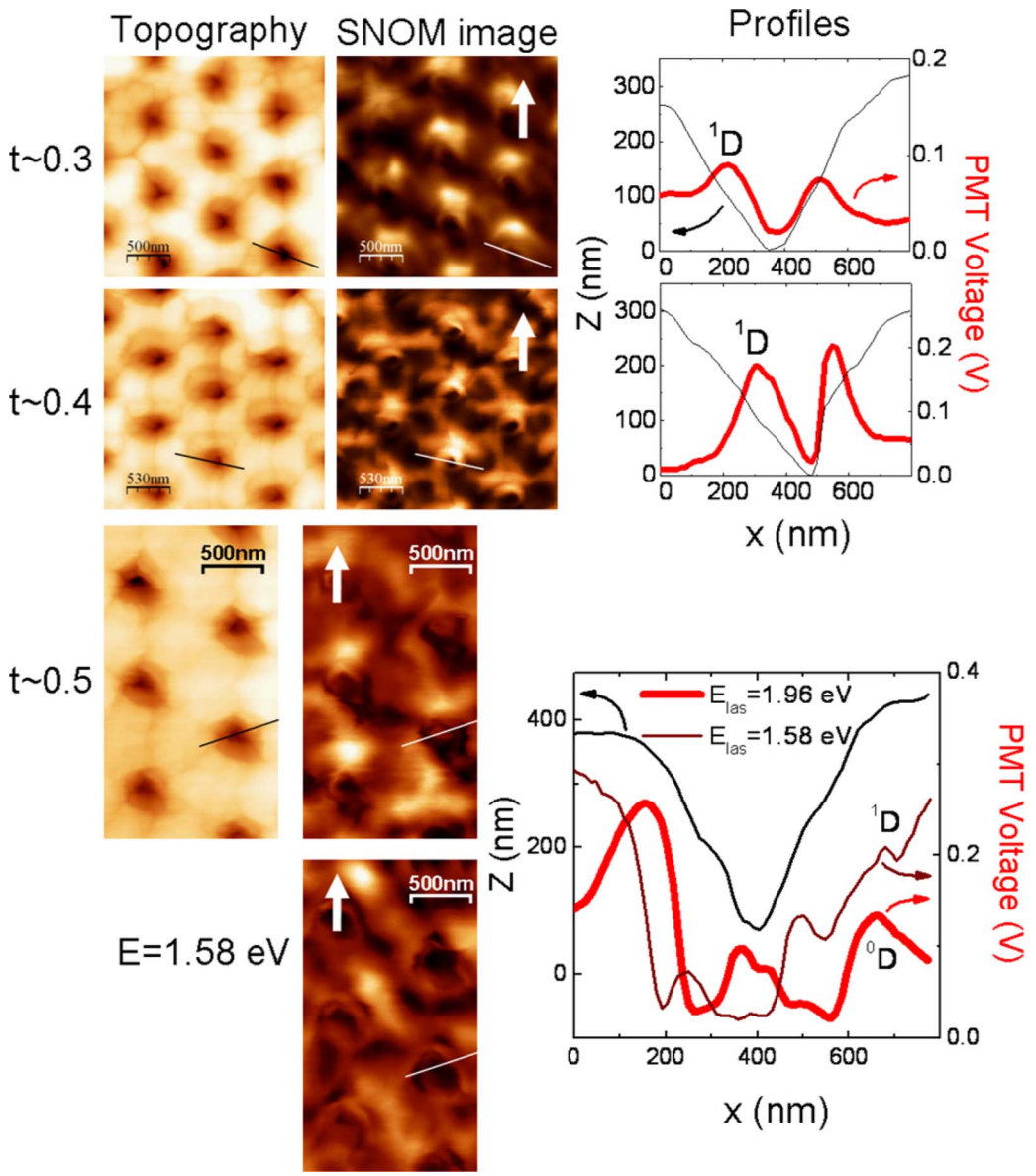

FIG. 4. (Color online) Topography and SNOM images of the $R=400$ nm void array at increasing normalized thickness, with (right) their corresponding profiles along the bars marked on the images. The white arrows indicate the direction of illumination in SNOM. The $E=1.96$ eV laser line was used for illumination at $t\sim0.3$ and $t\sim0.4$. For $t\sim0.5$ SNOM images taken with $E=1.96$ eV and $E=1.58$ eV are compared. In the latter case, both SNOM images were measured by switching the laser line without retracting the tip from the surface, i.e., it remained in feedback.

vation of the ^0D plasmon mode which for $t=0.5$ is well in resonance with the 1.96 eV laser line [see Fig. 3(b)]. We point out that the ^1F mode is another possible candidate for the assignment of this void plasmon. According to boundary element calculations, the ^1F mode is also close in energy at this truncation degree and displays a field distribution with a central maximum and side lobes, which matches SNOM features as well. Compelling evidence that the perturbation caused by the SNOM tip is not hampering the observation of the void modes is obtained when SNOM images for $t=0.5$ are also taken with a different laser line (1.58 eV) without retracting the tip from the feedback position. Hence, we measure exactly the same sample area under exactly the same conditions except for the different excitation energy. The results are shown in Fig. 4. In clear contrast to 1.96 eV light illumination, for near IR excitation at 1.58 eV a node develops at the void center and a ring-shaped profile is observed, similar to that observed for $t=0.3$ and 0.4 but with 1.96 eV excitation. Based on our reflectivity measurements and calculations we attribute this pattern to the $^1D^+$ mode, which becomes resonant for near IR excitation at a truncation degree of $t=0.5$ [Fig. 3(b)]. The fact that some SNOM images do not show an exact mirror symmetry with respect to a vertical mirror line for individual voids is mainly due to the asymmetries of the tip. In fact, the asymmetries are also present in the topography images. The cavity features of the SNOM images obtained upon scanning of areas with $t>0.5$ become smeared out. The topography images start to

show clear evidence of the formation of hexagonal arrays of mounds surrounding the entrance of each void, which close the void for increasing t.[17] Thus, the SNOM tip enters only partially into the cavities being unable to properly sense the electromagnetic field distribution inside the voids.

Despite the quite good agreement between measured and calculated void plasmon features there are some discrepancies which deserve some discussion. First, Mie modes with azimuthal component $m=0$ require p-polarized light to be excited. However, the ${}^0P$ void mode was observed in SNOM and reflectivity measurements as well, both performed with mainly s-polarized light. We suggest a polarization scrambling intrinsic to the nanovoid array as a probable explanation. Second, regarding the intensity distribution of the ${}^1D$ mode, the calculations predict not a ring but a dipolelike shape along the polarization of the incident laser. We believe that the latter is a consequence of multiple reflections between tip and inner cavity walls. At this stage, we would like to point out that the mode assignment of the resonant SNOM and reflectivity measurements, for which the boundary element calculations have proved to be extremely helpful, should be considered as preliminary. For a stringent comparison with the experiment it would be necessary to simulate the field distribution captured by a tip with similar parameters as the real one while it performs a scan over the void structure. At present, however, calculations can be carried out only for few fixed positions of the tip inside a void using a simplified model of the tip.

IV. CONCLUSIONS

In conclusion, we have reported the direct observation of the near-field spatial distribution of cavity plasmon modes in truncated gold void arrays by resonant SNOM with nanometer scale resolution. We have identified several cavity modes which show up as plasmon resonances in reflectivity spectra by systematically studying the dependence of the measured near-field distributions on the degree of truncation and excitation energy. Interestingly, we find that geometrical characteristics and overall symmetry of the observed field distributions are well accounted for by results of boundary element calculations allowing for a tentative void-mode assignment. Our experiments demonstrate that, in general, the SNOM technique is well suitable to yield direct insight into the plasmon-field enhancements in open metallic nanostructures. This is key information for the proper design of substrates to be used in applications such as optical spectroscopy with single-molecule sensitivity. In particular, our results suggest that a SNOM version of SERS might be possible in the nanovoid geometry.

ACKNOWLEDGMENTS

A.R.G. is an ICREA Research Professor. P.D.L. acknowledges an I3P-CSIC grant. SNOM measurements were performed at the Nanotechnology Laboratory of MATGAS 2000 A.I.E.

*placharmoise@icmab.es

[1] W. L. Barnes, A. Dereux, and T. W. Ebbesen, Nature (London) **424**, 824 (2003).
[2] A. Zayats and I. Smolyaninov, J. Opt. A, Pure Appl. Opt. **5**, S16 (2003).
[3] A. Krasavin, A. Zayats, and N. Zheludev, J. Opt. A, Pure Appl. Opt. **7**, S85 (2005).
[4] J. J. Baumberg, T. A. Kelf, Y. Sugawara, S. Cintra, M. Abdelsalam, P. N. Bartlett, and A. Russell, Nano Lett. **5**, 2262 (2005).
[5] T. A. Kelf, Y. Sugawara, J. J. Baumberg, M. Abdelsalam, and P. N. Bartlett, Phys. Rev. Lett. **95**, 116802 (2005).
[6] R. M. Cole, J. J. Baumberg, F. J. Garcia de Abajo, S. Majan, M. Abdelsalam, and P. N. Bartlett, Nano Lett. **7**, 2094 (2007).
[7] S. I. Bozhevolnyi, V. S. Volkov, E. Devaux, and T. W. Ebbesen, Phys. Rev. Lett. **95**, 046802 (2005).
[8] S. I. Bozhevolnyi, V. S. Volkov, E. Devaux, J. Y. Laluet, and T. W. Ebbesen, Nature (London) **440**, 508 (2006).
[9] P. N. Bartlett, J. J. Baumberg, P. Birkin, M. Ghanem, and M. Netti, Chem. Mater. **14**, 2199 (2002).
[10] P. N. Bartlett, J. J. Baumberg, S. Coyle, and M. Abdelsalam, Faraday Discuss. **125**, 117 (2004).
[11] J. Kim and K. B. Song, Micron **38**, 409 (2007), and references therein.
[12] S. C. Hohng, Y. C. Yoon, D. S. Kim, V. Malyarchuck, R. Müller, Ch. Lienau, J. W. Park, K. H. Yoo, J. Kim, H. Y. Ryu, and Q. H. Park, Appl. Phys. Lett. **81**, 3239 (2002).
[13] G. Ctistis, P. Patoka, X. Wang, K. Kempa, and M. Giersig, Nano Lett. **7**, 2926 (2007).
[14] B. Hecht, B. Sick, P. Wild, V. Deckert, R. Zenobi, O. J. F. Martin, and D. U. Pohl, J. Chem. Phys. **112**, 7761 (2000), and references therein.
[15] L. Novotny, D. W. Pohl, and B. Hecht, Ultramicroscopy **61**, 1 (1995).
[16] D. Richards, Philos. Trans. R. Soc. London, Ser. A **361**, 2843 (2003), and references therein.
[17] T. A. Kelf, Y. Sugawara, R. M. Cole, J. J. Baumberg, M. E. Abdelsalam, S. Cintra, S. Mahajan, A. E. Russell, and P. N. Bartlett, Phys. Rev. B **74**, 245415 (2006).